Impact of Distal Side Water and Residue 315 on Ligand Binding to Ferric *Mycobacterium tuberculosis* Catalase−Peroxidase (KatG)[†]

Kalina Ranguelova,[‡,§] Javier Suarez,[‡,||] Leonid Metlitsky,[‡] Shengwei Yu,[‡] Shelly Zev Brejt,[‡] Sidney Zelig Brejt,[‡] Lin Zhao,[⊥] Johannes P. M. Schelvis,[⊥,#] and Richard S. Magliozzo*[,‡,||]

Department of Chemistry, Brooklyn College, 2900 Bedford Avenue, Brooklyn, New York 11210, Department of Biochemistry, The Graduate Center of the City University of New York, 365 Fifth Avenue, New York, New York 10016, and Department of Chemistry, New York University, 31 Washington Place, New York, New York 10003

Received August 11, 2008; Revised Manuscript Received September 25, 2008

ABSTRACT: The catalase−peroxidase (KatG) of *Mycobacterium tuberculosis* (*Mtb*) is important for the virulence of this pathogen and also is responsible for activation of isoniazid (INH), an antibiotic in use for over 50 years in the first line treatment against tuberculosis infection. Overexpressed *Mtb* KatG contains a heterogeneous population of heme species that present distinct spectroscopic properties and, as described here, functional properties. A six-coordinate (6-c) heme species that accumulates in the resting enzyme after purification is defined as a unique structure containing weakly associated water on the heme distal side. We present the unexpected finding that this form of the enzyme, generally present as a minority species along with five-coordinate (5-c) enzyme, is the favored reactant for ligand binding. The use of resting enzyme samples with different proportional composition of 5-c and 6-c forms, as well as the use of KatG mutants with replacements at residue 315 that have different tendencies to stabilize the 6-c form, allowed demonstration of more rapid cyanide binding and preferred peroxide binding to enzyme containing 6-c heme. Optical-stopped flow and equilibrium titrations of ferric KatG with potassium cyanide reveal complex behavior that depends in part on the amount of 6-c heme in the resting enzymes. Resonance Raman and low-temperature EPR spectroscopy clearly demonstrate favored ligand (cyanide or peroxide) binding to 6-c heme. The 5-c and 6-c enzyme forms are not in equilibrium on the time scale of the experiments. The results provide evidence for the likely participation of specific water molecule(s) in the first phases of the reaction mechanism of catalase−peroxidase enzymes.

A complete understanding of how structure relates to function in monofunctional heme catalases and peroxidases remains a complex and interesting problem in enzymology. For the dual function catalase−peroxidase (KatG)[1] enzymes found in microorganisms, a unique structural feature responsible for establishing catalase activity in this class I peroxidase is a three amino acid adduct in which the side chains of distal residues Met255, Tyr229, and Trp107 are covalently linked. Other residues in the KatG enzymes have been assigned specific roles for enzyme stability, substrate access and binding, and roles specific to catalytic functions, though the detailed analysis of such features is in its early stages.

The KatG of *Mycobacterium tuberculosis* (*Mtb*) is important for the virulence of this pathogen because of its role in the removal of peroxide in infected host macrophage (*1*−*3*). It also plays a direct role in activation of the antibiotic, isoniazid (INH), a pro-drug in use for over 50 years as part of the first line treatment modalities against TB infection. The growing worldwide problem of resistance to this drug due to mutations in the *katG* gene has been addressed in clinical and biochemical studies often focused on mutations at the 315 position, with KatG[S315T] being the mutant most commonly found in isoniazid resistant bacteria (*4, 5*). The loss of high-affinity INH binding in this mutant was recently presented as an explanation for INH resistance; the methyl group of the threonine residue restricts a narrow opening at the bottom of a substrate access channel leading from the surface of the enzyme to the heme edge at the propionate of pyrrole IV, which was considered the structural change explaining the poor interactions between the mutant and INH (*5*). In this example, INH resistance does not simply derive from a general loss in catalytic capacity because only moderate reductions in its catalase reaction rate, the rate of peroxidation of artificial substrates other than INH, and in the rate of formation of compound I from resting enzyme with alkyl peroxides has been found (*6*). The importance of residue 315 in high-affinity drug binding became more evident with the publication of a crystal structure of CcP in

[†] This work was supported by NIH Grant AI060014 (NIAID) to R.S.M.

* Corresponding author. E-mail: rmaglioz@brooklyn.cuny.edu.
[‡] Brooklyn College.
[§] Current address: Laboratory of Pharmacology, National Institute of Environmental Health Sciences, National Institutes of Health, P.O. Box 12233, MD F0-01, 111 TW Alexander Drive, Research Triangle Park, NC 27709.
[||] The Graduate Center of the City University of New York.
[⊥] New York University.
[#] Current address: Department of Chemistry and Biochemistry, Montclair State University, Montclair, NJ 07043.

[1] Abbreviations: KatG, catalase−peroxidase; *Mtb*, *Mycobacterium tuberculosis*; INH, isonicotinic acid hydrazide (isoniazid); EPR, electron paramagnetic resonance; 5-c, five coordinate; 6-c, six coordinate; QS, quantum spin; LS, low spin; CcP, cytochrome *c* peroxidase.

10.1021/bi801511u CCC: $40.75
Published on Web 10/29/2008

complex with INH (*7*). In this class I peroxidase and presumably in KatG as well, hydrogen bonds between serine 185 (315 in *Mtb* KatG), a water molecule, and the pyridine nitrogen of the drug are among the interactions that provide specific binding of INH within the heme pocket near the δ-heme edge. Thus, replacements at residue 315 of KatG are expected to interfere with drug binding and activation in general as for KatG[S315T], without broadly compromising heme structure and function.

The KatG[S315T] mutant is generally interesting because enzyme functions are preserved despite the poor interaction with INH, thereby preserving bacterial physiology and virulence (*8*). Our prior reports on its structure and function demonstrated that this mutant exhibits a strong preference for 5-c heme over the 6-c heme species that accumulates in WT KatG after purification (*6, 9*). The potential impact of this heterogeneity upon catalytic function in KatG led to the examination here of the binding of cyanide as a surrogate for the initial steps in peroxidase turnover. Compound I formation from ferric heme enzymes passes through a precursor, compound 0, which is a 6-c low-spin species in which peroxide is bound to iron at the sixth coordination position. This complex is too short-lived for observation in WT KatG by conventional stopped-flow measurements (*10, 11*). The route to compound 0 involves diffusion of peroxide to the active site and its deprotonation to allow anion binding to heme iron. The ligation of cyanide proceeds through a similar process.

We present the unexpected finding that a 6-c KatG enzyme form is a preferred reactant with cyanide (and alkyl peroxide) and suggest that distal water molecule(s) play a facilitating role in the ligand binding mechanism. We had previously determined from X-ray crystal structures that structured water in the active site is more abundant in WT KatG than in KatG[S315T] (*5*). For the purified enzymes in solution, 6-c heme is evident in unique optical, resonance Raman, and EPR spectra for this species, which accumulates during brief storage of the purified enzyme. Five-coordinate forms predominate in the freshly isolated enzymes (*4, 5*), and the abundance of the 6-c species and the rate at which they appear vary in the S315 mutants examined here.

Rationale for investigating these issues in overexpressed *Mtb* KatG comes from the observation that the enzyme isolated from *Mtb* cells is heterogeneous in terms of coordination number of heme iron (*12*) just as we find for the overexpressed enzyme. Changes in coordination number, which are extremely slow in KatG[S315T], are found here to be very rapid in KatG[S315G], also a drug-resistant mutant (*13*), and KatG[S315C]. The three mutants provided a variety of resting enzyme species upon which comparisons and interpretation of ligand binding could be based. Our results illustrate properties not recognized before in KatG and suggest that descriptions of the reaction mechanism of catalase−peroxidases should include a water molecule as a participant in the proton transfers/isomerizations within the distal cavity that accompany the initial steps in both catalase and peroxidase turnover.

EXPERIMENTAL PROCEDURES

Chemicals and Reagents. KCN and other reagents were purchased from Sigma-Aldrich or Fisher Scientific and were used without further purification.

Construction, Expression, and Purification of the S315T, S315G, and S315C Mutants of KatG. The plasmid pKAT II was used as an overexpression vector for KatG as well as a mutagenesis template. *Escherichia coli* strain UM262 was used for overexpression (*1, 2, 14, 15*). UM262 and pKAT II were both gifts from Stewart Cole (Institut Pasteur, Paris). Mutagenesis was performed using the QuickChange II site-directed mutagenesis kit from Stratagene (La Jolla, CA). The pairs of complementary primers (synthesized and purified by Operon Biotechnologies, Inc.) were designed to introduce the required mutation. The oligonucleotide pairs (mutated codons are in bold) were as follows: S315T, 5′-^{925}GGTAAGGACGCGATCAC-C**GGC**GGCATCGAGGTCG^{958}-3′ and 5′-^{958}CGACCTCGAT-GCC**GCC**GGTGATCGCGTCCTTACC^{925}-3′ (*6*); S315G, ^{925}GG-TAAGGACGCGATCACC**GGC**GGCATCGAGGTCG^{958}-3′ and 5′-^{958}CGACCTCGATGCC**GCC**GGTGATCGCGTC-CTTACC^{925}-3′; and S315C, 5′-^{925}GGTAAGGACGCGATCAC-C**TGC**GGCATCGAGGTCG^{958}-3′ and 5′-^{958}CGACCTCGAT-GCC**GCA**GGTGATCGCGTCCTTACC^{925}-3′. Mutagenesis was performed according to the manufacturer's protocol, and the reaction products were transformed into the *E. coli* XL1-Blue strain for selection purposes. The presence of the mutated 315 codon in the *katG* gene was confirmed by DNA sequencing (Gene Wiz, Inc.), and the mutated plasmid was electroporated into *E. coli* strain UM262 for protein overexpression.

All KatG enzymes were purified from freshly collected cultures, as previously described (*16*), in potassium phosphate buffer, pH 7.2. The pure enzymes had optical purity ratios (A_{405}/A_{280}) of ~0.5 for WT KatG and KatG[S315C] and ~0.45 for KatG[S315T] and KatG[S315G].

EPR Spectroscopy. Low-temperature X-band EPR spectra were recorded using a Bruker E500 EPR spectrometer equipped with an Oxford Spectrostat continuous-flow cryostat and ITC503 temperature controller. EPR data acquisition and manipulation were performed using XeprView and WinEPR software (Bruker). The spectra of ferric proteins (100 μM) were recorded in 20 mM potassium phosphate buffer, pH = 7.2, at 4 K. For spectra of the cyanide forms, ferric KatG was incubated with potassium cyanide (KCN) and then frozen in liquid nitrogen after 30 min. Quantification of EPR signals was based on a sample of the horse heart metmyoglobin−CN complex of known concentration prepared by addition of excess KCN (10:1 molar ratio) to Mb in 20 mM phosphate buffer (pH 7.2). The concentration of the Mb−CN complex was based on the intensity of the band at 542 nm (ε = 8.7 $mM^{-1}\cdot cm^{-1}$) (*17*). Estimation of the concentrations of 5- and 6-c KatG species was based upon the integrated EPR signal intensities normalized according to *g*-value differences (*18*) of KatG samples of known concentrations, with simulation of experimental spectra as the sum of spectra of the individually identified species as in the approach in ref *19*. The relative abundance of three species in EPR spectra (r_1, r_2, and r_3 signals) based on this approach was similar to the reported abundance based on room temperature resonance Raman analysis given in ref *9* for similar samples of KatG and KatG[S315T].

Resonance Raman Spectroscopy. Enzyme samples (50 μM KatG in 20 mM potassium phosphate buffer, pH 7.2) for resonance Raman experiments were held in a spinning cell sealed with a rubber septum. The cyanide adducts of KatG were prepared by adding concentrated potassium cyanide buffered to pH 10 using sodium borate into the cell to give final concentrations of cyanide equal to 0.5 mM for WT KatG or 0.5 M in the case of KatG[S315T] to obtain complete conversion in a reasonable time period. Resonance Raman (RR) spectra were obtained using a single spectrograph (TriAx 550, JY/Horiba) and a N_2(l)-cooled CCD detector (Spectrum One, JY/Horiba) with a UV-enhanced 2048 $\times$ 512 pixel chip (EEV). Toluene was used for wavenumber calibration, and the spectral resolution was 4 cm^{-1} with peak positions determined to within 1 cm^{-1}. The samples were excited with 413.1 nm light from a Kr^+ laser (Coherent, I-302) with an incident laser power of 10 mW and were kept at 6 $\pm$ 2 °C during data collection. Rayleigh scattering was removed with a 413.1 nm holographic notch filter (Kaiser Optical). Background correction of spectra was performed by subtraction of a smooth polynomial. Raman bands were assigned according to refs *20*−*22*. To determine relative peak intensities and positions within the ν_3-region where overlapping bands are found (*23*), the 1470 to 1520 cm^{-1} spectral region was fit to Lorentzian line shapes with bandwidths of 13.5 cm^{-1} as described previously (*9*).

Electronic Absorption and Stopped-Flow Spectrophotometry. Spectrophotometric experiments were performed using an NT14 UV−vis spectrophotometer (Aviv Associates, Lakewood, NJ). Optical spectra were recorded in 20 mM potassium phosphate buffer, pH 7.2, using 5−6 μM enzyme (heme concentration). Titrations with cyanide were performed by adding 1−1.2 μL aliquots of potassium cyanide stock solutions to 1 mL of enzyme held in a cuvette. After each portion of cyanide was added, the solution was thoroughly mixed, and the spectrum was recorded after 20 min to ensure completion of the binding reaction. The data were fit using SigmaPlot (SYSTAT) software.

A stopped-flow apparatus (HiTech Scientific Model SF-61DX2) was used to evaluate the kinetics of cyanide binding to resting enzymes. For evaluation of cyanide binding rates as a function of pH (5.5, 7.2, and 9.5), enzymes were mixed with a 25-fold molar excess of ligand under conditions that maintained the concentration of free HCN (and the ionic strength) constant by adjustment of the buffer and total potassium cyanide concentrations. Data acquisition and analysis utilized Kinet-Asyst software (HiTech Scientific). Observed pseudo-first-order rates were plotted as a function of cyanide concentration to obtain second-order rate constants for cyanide binding. The k_{obs} values were fit to the expression $k_{obs} = k_{on}[CN] + k_{off}$, where k_{on} is the rate of binding and k_{off} is the rate of dissociation. Biphasic cyanide binding was observed for all enzymes, and the observed rates were linearly dependent upon cyanide concentration. Separate linear plots for the fast and the slow components were created from the k_{obs} values obtained from the optical data. The slopes of these plots give the apparent second-order association rate constants for two phases of cyanide binding.

The time course of cyanide binding was also observed by following the change in absorbance at 405 nm and at 420 or 423 nm for WT KatG and the KatG[S315T] mutant in the presence of excess cyanide similar to the Raman time course experiments. Such data were fitted using the equation $A = A_0 + B_1(1 - \exp(-t/\tau'_{1/2})) + B_2(1 - \exp(-t/\tau''_{1/2}))$, where B_1 and B_2 are the amplitudes of both phases and $\tau'_{1/2}$ and $\tau''_{1/2}$ are the time constants, respectively.

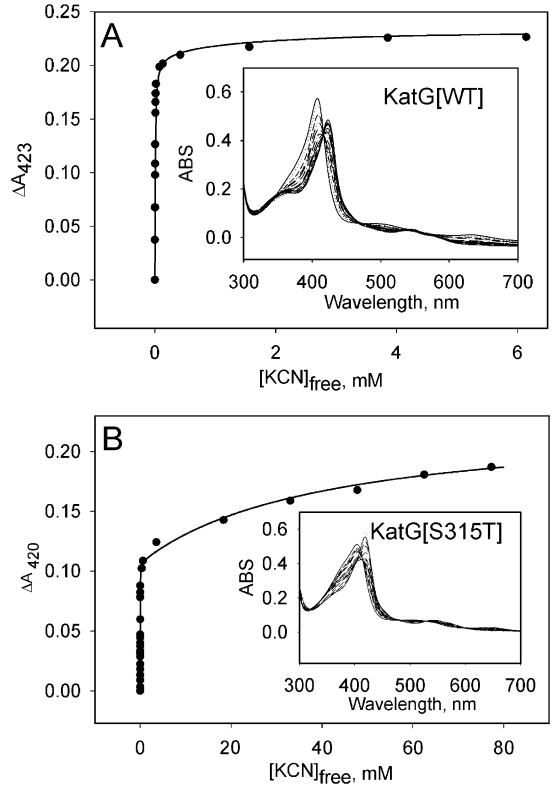

FIGURE 1: Titration of wild-type KatG (panel A) and KatG[S315T] (panel B) with potassium cyanide. The data points on the plots show ΔA_{423nm} (or ΔA_{420nm} for the mutant) values as a function of the concentration of free cyanide. The data were fit to a two binding site (noninteracting) model yielding K_{D1} and K_{D2} values equal to 6.8 μM and 1.5 mM for WT KatG and 10 μM and 40 mM for KatG[S315T]. The insets show full spectra of the enzymes recorded 20 min after each addition of cyanide.

RESULTS

Cyanide Titrations. Figure 1 shows ligand binding curves based on a conventional optical titration of freshly isolated WT KatG (panel A) and KatG[S315T] (panel B). A shift in the Soret absorbance from 405 nm to either 423 nm (for wild type) or 420 nm (for KatG[S315T]), a new band appearing at 540 nm, and the disappearance of the CT1 and CT2 bands (around 640 and 500 nm, respectively) characterize conversion to the 6-c LS cyanide complexes. After a small molar excess of cyanide was added, much larger excesses of ligand were required to complete the titrations, especially in the case of KatG[S315T]. A proportion of heme remained ligand free when an apparent plateau had been reached in the titration as demonstrated by EPR spectroscopy showing that, in the presence of as much as a 100-fold molar excess of cyanide, the enzyme still exhibited significant intensity of signals around $g = 6$ from the resting ferric enzyme (not shown). This confirmed that binding to a high-affinity species was completed without conversion of all the heme into the 6-c LS cyanide complex, rather than a process such as an isomerization or other reaction that alters the optical properties of the 6-c LS cyanide complex at high ligand concentration.

Table 1

KatG	K_{D1}	K_{D2}
WT	6.8 μM	1.5 mM
S315T	10 μM	40 mM
S315G	0.13 μM	3.45 μM
S315C	<1 nM	2.3 μM

No change in optical properties was observed for the 6-c LS complex as a function of increased ionic strength (not shown). In order to establish whether HCN or CN^- is the species binding to heme, we evaluated the on-rates for ligand binding at pH 5.5, 7.2, and 9.5, in each case using conditions that maintained constant ionic strength and a constant concentration of available HCN. This approach showed only a very small difference in binding rate at the three pH values (not shown) and demonstrated that HCN is the liganding species.

In stark contrast to the titrations of WT KatG and KatG[S315T], KatG[S315G] and KatG[S315C] mutants could be completely titrated to the 6-c LS cyanide complex with just a small molar excess of cyanide (Supporting Information, S1).

Dissociation constants were evaluated from the titration data analyzed for two noninteracting binding sites (Figure 1, Table 1). The K_D values obtained for KatG[S315G] and KatG[S315C] were significantly lower than for WT KatG and KatG[S315T], and there was a smaller difference between the affinity constants for the two binding steps.

These results demonstrate that there are at least two binding processes for each enzyme. The fraction of total enzyme titrated in the higher affinity process was approximately 80% for both WT KatG and KatG[S315G]. This distribution was closer to 50:50 in the case of KatG[S315T] and approximately 65:35 for KatG[S315C]. Interestingly, freshly isolated KatG[S315T] contains two 5-c heme forms (high spin and quantum spin) in nearly equal proportions (*9*). The equal proportions for two phases of the titration for this mutant could be considered evidence for large differences in affinity for the two 5-c species, or for strong anticooperativity in the ligand binding process such that once one heme group is titrated to low spin, the second heme in the same dimer molecule shifts to (or inherently has) low affinity. The distribution of the two phases of binding in the other KatG enzymes, which do not correspond to any known structural features, however, argues against these ideas (*9, 24*).

Stopped-flow spectrophotometry provided k_{on} and k_{off} rates evaluated under pseudo-first-order conditions and allowed confirmation that high-affinity binding reflects rapid k_{on} and very slow k_{off} rates. Rates (Supporting Information, S2) and the calculated K_D values based on these rates are presented in Table 2. The high ratio of k_{on} over k_{off} determines the high ligand affinities and shows that greatly decreased k_{on} values are responsible for the low-affinity binding process. Values for the equilibrium dissociation constants (K_D) were calculated from the ratios of k_{off} to k_{on}. These K_D values compare reasonably well with those obtained by equilibrium titration of WT KatG and the value for the first phase in the S315T mutant shown in Figure 1 (but not the second). The discrepancy may arise because the k_{off} values are not very accurately determined in this approach because of the very slow rates giving intercepts at zero ligand concentration close to zero. The important observation here is that high- and low-affinity binding arises from differences in on-rates.

Knowledge that resting KatG contains at least three different species according to previous resonance Raman, optical, and EPR evidence (*9*) suggested that these titrations may not reveal underlying small differences in ligand affinity among these species. Therefore, the titration process was reexamined using very small (0.03) molar equivalents of cyanide for the ligand addition steps. A third binding process was in fact detected in this approach, most clearly for WT KatG. A steeper slope in the curve during addition of the first 0.5 equiv of ligand was found, and this phase was followed by two lower affinity processes. In the more conventional titration above, these differences were not resolved when larger ligand additions were made. For KatG[S315T], there was hardly any detectable difference between the slopes during the very early phase compared to the rest of the titration in this approach. These data (Supporting Information, S3) were not analyzed further but are consistent with preferential titration of a species present in low abundance in the resting enzymes which is not in equilibrium with other forms. EPR and resonance Raman experiments described below provide insights into the origins of this behavior as preferential binding to 6-c forms of the enzymes.

Resonance Raman Spectroscopy. Resonance Raman spectroscopy provided direct evidence for favored binding of cyanide to 6-c enzyme in KatG[S315T]. The partially resolved ν_3 bands which are sensitive to spin state and coordination number were previously described for ferric 5-c HS, 5-c QS, and 6-c heme in both WT KatG and KatG[S315T] (*9, 24*). EPR spectroscopy also distinguishes three principal species in these resting enzymes (see below). The distribution of species in the fresh resting KatG[S315T] enzyme was approximately 10% 6-c heme (1487 cm^{-1}) and ~90% 5-c heme (sum of the band intensities at 1495 and 1503 cm^{-1}). Changes in the ν_3 band intensities were followed after addition of a large excess of cyanide. The first spectrum recorded after addition of ligand was collected 3 min after mixing (the time necessary to obtain a spectrum with adequate signal-to-noise ratio for band deconvolution), and spectra were recorded at 15 min intervals until conversion to the cyanide complex was complete (Figure 3). As expected, a new band characteristic of 6-c ferric low spin heme appears (at 1510 cm^{-1}), while the bands of the resting enzyme species (at 1487, 1503, and 1495 cm^{-1}) decrease in intensity. The new population distribution immediately after addition of cyanide was comprised of 80% 5-c forms and 20% 6-c LS heme; the band at 1487 cm^{-1} had already been abolished in the first spectrum collected after addition of cyanide, consistent with rapid elimination of the 6-c heme species. Subsequent spectra showed similar rates of disappearance of the two 5-c species. Time constants for the two processes had values estimated at 3 min and 91 $\pm$ 9 min. The isolated observation of ligand binding favoring 6-c heme was confirmed using EPR spectroscopy (see below). In the case of WT KatG (not shown), no favored loss for any of the bands was resolved under these conditions.

In an analogous experimental approach using conventional spectrophotometry, a large excess of cyanide was added to the resting enzymes, and sequential spectra were recorded. A rapid and slow binding process could be resolved for WT

Table 2[a]

	k_{1on} (M^{-1} s^{-1})	k_{2on} (M^{-1} s^{-1})	k_{1off} (s^{-1})	k_{2off} (s^{-1})	K_{D1} (μM)	K_{D2} (mM)
WT	1.3×10^6	1.4×10^3	9.0	1.3	6.9	0.9
KatG[S315T]	3.9×10^5	2.8×10^2	3.9	0.3	10	1.1
KatG[S315G]	9.5×10^5	1.2×10^3	8.1	0.15	8.5	0.13

[a] The KatG samples for these experiments had been stored at 4 °C for 4 weeks and contained somewhat greater proportions of 6-c heme, but these data were not analyzed in the context of this structural heterogeneity. The "aging" of KatG has been described before (*24*).

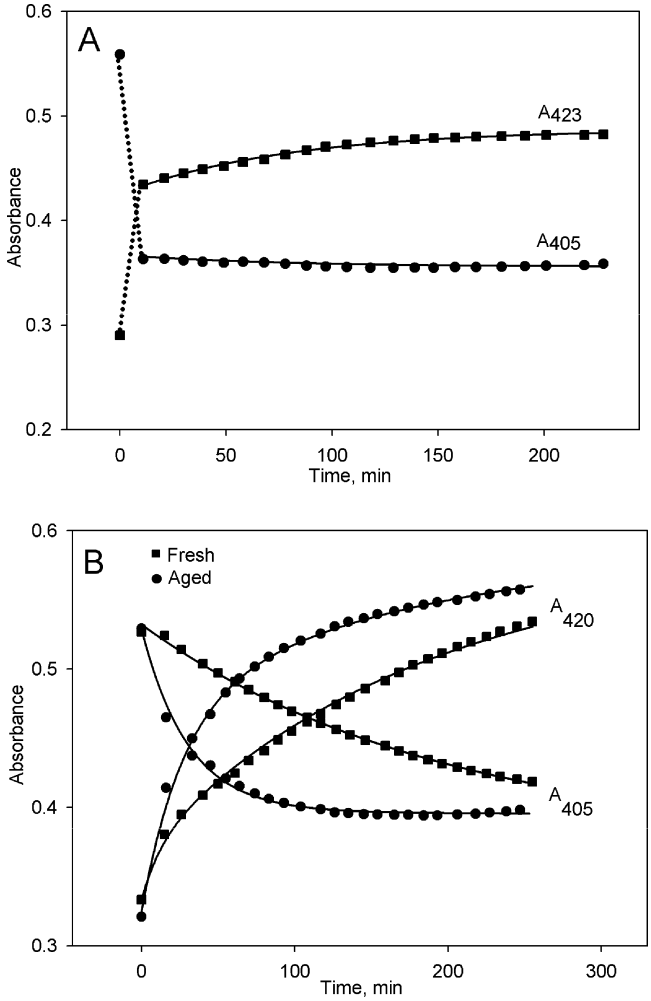

FIGURE 2: Time course of titration of wild-type KatG and KatG[S315T] with cyanide. (A) 5 μM WT KatG was mixed with 5 mM KCN and the change in absorbance at 405 nm (circles) (to monitor the loss of resting enzyme) and 423 nm (squares) (to monitor the increase in 6-c LS heme) was plotted The data were fit to a monoexponential decay or growth function (time constant of 79 min) after eliminating the first data point. (B) 5 μM (freshly isolated or "aged") KatG[S315T] was mixed with 50 mM KCN, and the change in absorbance was plotted as above. The data were fit to biexponential decay or growth functions with time constants of 12 and 181 min for the fresh enzyme and 27 and 177 min for the "aged" enzyme.

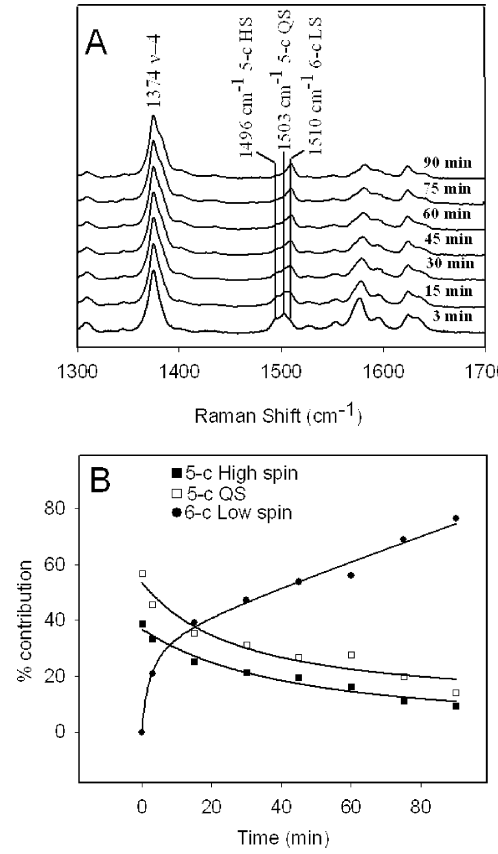

FIGURE 3: (A) High-frequency resonance Raman spectra of KatG[S315T] at different time points after addition of 0.5 M KCN. The excitation wavelength was 413.1 nm. The frequency, spin state, and heme iron coordination numbers are given for each of three ν_3 bands in the region near 1500 cm^{-1}. (B) Time course of the change in intensity for the three ν_3 bands in the region near 1500 cm^{-1}. The solid lines are biexponential fits to the data with time constants of 2.9 and 91 min in each plot.

KatG in the presence of 5 mM total potassium cyanide and for KatG[S315T] plus 50 mM KCN (the large excesses used in order to achieve complete ligand binding in reasonable[2] time periods). A plot of the absorbance at 405 nm (or 420/423 nm) revealed biphasic kinetics for both WT KatG and KatG[S315T] (Figure 2). For WT KatG, the first phase of complex formation was complete by the time the first spectrum could be recorded (Figure 2A). To evaluate a rate for the second phase (starting after 10 min), the first data point after cyanide addition was omitted, and the remaining data were fit to a single exponential growth curve. The calculated time constant was 79 min. The important issue here is that the first phase consumed a fraction of the total enzyme ultimately converted to the 6-c LS complex by cyanide. In the case of KatG[S315T], the rates were slower, and individual time constants could be evaluated. Despite the apparent presence of more than two species with different affinities found in the equilibrium titration using small fractional equivalents of ligand, this approach did not reveal three processes because of the presence of excess ligand that achieves combined titration of the higher affinity binding forms without resolving a difference. This optical experiment

[2] Under conditions where the cyanide concentration is similar to or exceeds the buffer concentration in the case of KatG[S315T] titration, pH control is lost, and the resulting titration data for the second K_D value may be considered valid for the affinity at alkaline pH (>9). In any case, the "break" in the titration curves is in a region where the pH is still controlled by the buffer concentration, and the key observation here is that there are two binding processes in each enzyme.

was not performed for KatG[S315G] or S315C mutants due to the small amount of cyanide needed to achieve saturation and the near equivalence for two binding processes described above.

Interestingly, and as would be predicted based on the evidence above for KatG[S315T], the time courses for the binding of cyanide varied for resting enzyme that contained nearly exclusively 5-c heme iron, as found in freshly isolated enzyme, compared to resting ("aged") enzyme that had a larger proportion of 6-c heme iron. To illustrate the phenomenon clearly, results are compared for enzyme that had been stored for 1 month and freshly isolated enzyme (*9, 24*). Figure 2B shows that a larger proportion of total optical change occurred at a fast rate for the aged enzyme sample compared to the time course using the fresh enzyme. The data were fit to a biphasic exponential growth model with time constants equal to 12 and 181 min for the fast and slower phases for the fresh enzyme and 27 and 177 min for the aged enzyme. Note that the amplitude of the fast phase is a small fraction of the total optical change for the fresh enzyme and is less accurately evaluated. The time constants for the slow phase are reasonably well matched for the experiments using aged and fresh enzyme samples, consistent with the presence of the same slower reacting species in both samples but an increase in the amount of the faster reacting species in the aged enzyme. These results provided further evidence for binding processes that vary with the relative abundance of 6-c enzyme.

In the approaches using excess cyanide, the faster phase must have components of binding to both 6-c and some 5-c enzyme, while the slow phase is exclusively to the lowest affinity 5-c heme species shown in the Raman results.

EPR Spectroscopy. Before presenting the results of cyanide binding experiments, an analysis of EPR spectra of heme in resting WT, KatG[S315T], and KatG[S315G] enzymes is outlined. For each enzyme, two rhombic signals of different anisotropy are found (signal r_1, $g_1 = 6.30$, $g_2 = 5.09$ and $g_3 \sim 2$, and signal r_3, $g_1 = 6.68$, $g_2 = 5.09$, and $g_3 \sim 2$) which were previously assigned to 5-c heme iron species (*24, 25*). Here, and in our previous studies (*9, 24*), after storage of WT enzyme at 4 °C for periods beyond a few days, the r_1 signal decreases in intensity and another less anisotropic signal (r_2, $g_1 = 5.94$ and $g_2 = 5.49$) appears. Similar changes occur in KatG[S315T] but at a much slower rate (Figure 4) and were surprisingly found to occur at a much faster rate in KatG[S315G] and KatG[S315C] mutants, compared to WT KatG.

While EPR signals with $g_\perp$ close to 6 and axial or small rhombic splittings are routinely assigned to 6-c heme iron, we sought some confirmatory evidence for assignment of the r_2 signal to a specific structure in KatG. We considered that the species giving this signal might be an example of the QS spin state (rather than a 6-c HS heme) since we had assigned a 5-c QS heme species in freshly purified KatG (*26*) and there is similarity between the r_2 signal and the EPR spectrum reported for the benzohydroxamic acid (BHA) complex of HRPA2 (g-values of 5.93, 5.36, 1.99) and other complexes assigned as 6-c QS heme species (*26, 27*). X-ray crystallography shows that the HRP−BHA complex contains a distal water molecule 2.6 Å from heme iron. Similarly, the X-ray crystal structure of *Mtb* WT KatG contains an ordered water molecule 2.8 Å above heme iron (*5*). While these distances are long for typical metal−water ligand bonds, it is reasonable that a water molecule is also close to heme iron in frozen solutions and that this water perturbs the ligand field and or the porphyrin geometry giving rise to a unique EPR species in these analogous examples (*28*).

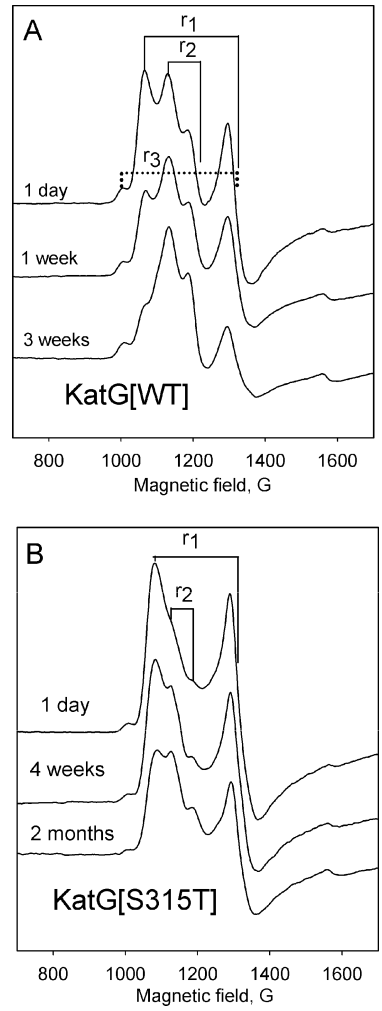

FIGURE 4: Assignment of EPR signals in low-temperature spectra of wild-type KatG (A) and KatG[S315T] (B). The features in the $g = 6$ region representing the different heme species for samples of the enzyme frozen after different periods of storage are indicated. Experimental conditions: temperature, 4 K; microwave power, 1 mW; modulation amplitude, 4 G; frequency, 9.3867 GHz.

Similarities between the HRPC−BHA example and the structure of *Mtb*KatG are also found when applying the normal-coordinate structural decomposition (NSD) analysis method based on X-ray coordinates (*29*). The saddling/ruffling heme deformation ratio for heme A in WT KatG was very close to that of the HRPC−BHA complex, suggesting that the similarity in EPR signals (r_2 vs the HRPC−BHA spectrum) arises from similar heme structure in these 6-c complexes. Therefore, we suggest that the r_2 signal is most consistent with a 6-c species that may be an example of a QS heme. The g-values for this signal fit the criterion of $4 > (g_1 + g_2)/2 < 6$ commonly used for such assignment (*30*).

Structural changes in KatG[S315T] were also documented in EPR spectra (Figure 4B) in the purified enzyme during storage. For this mutant, the predominating signals are the rhombic r_1 and r_3 signals described above, with slightly different g-values compared to the corresponding species in

wild type (r_1, $g_1 = 6.15$, $g_2 = 5.04$, and $g_3 = 1.97$, and r_2, $g_1 = 6.65$, $g_2 = 5.04$, and $g_3 = 1.97$). The r_2 signal grows in intensity but only after lengthy storage periods, being barely detectable in spectra of the fresh KatG [S315T] mutant and remaining lower in intensity compared to wild type after similar storage periods. For this reason, the mutant protein was examined during more than 4 weeks storage, to follow evolution of the r_2 signal and for easier illustration of the changes upon ligand binding. Interestingly, in the case of KatG[S315G] and KatG[S315C], the samples frozen for EPR within 1 day after purification exhibited the r_2 signal as the majority species (data not shown).

Given this framework for defining the EPR signals, we examined ligand binding under conditions where cyanide was added in limiting stoichiometry. Under such conditions, it was expected that preferential binding to the high-affinity (or quicker reacting) enzyme species would occur at the expense of the other species. Figure 5 shows the EPR spectra recorded for WT KatG and aged KatG[S315T] and S315G titrated with varying amounts of cyanide. A decrease in intensity of the r_2 signal was found for WT KatG in the presence of 0.1 mol equiv of cyanide, and the signal was abolished by addition of 0.5 equiv of cyanide. The r_1 signal and r_3 signals remain close to their starting intensities. The EPR signal characteristic of the 6-c LS cyanide complex appears as the cyanide concentration was increased ($g_{max} = 3.14$) (Figure 5A) as expected for ligand binding to heme iron. With higher concentrations of cyanide, the r_1 and r_3 signals also decreased in intensity as the 6-c LS signal increased. Similar results were found using aged KatG[S315T] (Figure 5B) for which complete titration of the r_2 signal occurred with 0.5 mol equiv of cyanide. Similar results were seen for freshly isolated KatG[S315G] (Figure 5C).

The favored binding of cyanide to the species giving the r_2 EPR signal is notable because the species is present in lowest abundance compared to the 5-c forms. Its relative abundance is estimated to be ~20% of total heme in the aged mutant sample, while for WT KatG aged for 1 week its concentration is ~30% of total heme. Selective titration of the minority species is unambiguous in the EPR results, while the absolute abundance of the starting species is not critical to our interpretation. In these experiments in which small amounts of CN were added to resting enzymes, no change in pH occurs, and the observed effects are therefore due to ligand binding only.

Larger excesses of cyanide were required to completely titrate the species giving the rhombic r_1 signal in both WT and S315T. This clearly confirms the assignment of the r_1 EPR signal to 5-c heme because the Raman results demonstrated that 5-c heme has lower affinity for cyanide.

A related experiment using stoichiometrically limiting peroxide demonstrated a phenomenon similar to that found using cyanide. Addition of 0.2 mol equiv of either peroxyacetic acid (PAA) or *tert*-butyl peroxide (*t*-BOOH) reduced the intensity of the r_2 signal for wild type and KatG[S315T], while the intensity of signals r_1 and r_3 remained constant (Figure 6). These observations demonstrate a favored reaction between peroxide and the species responsible for the r_2 signal in analogy to the behavior with cyanide.

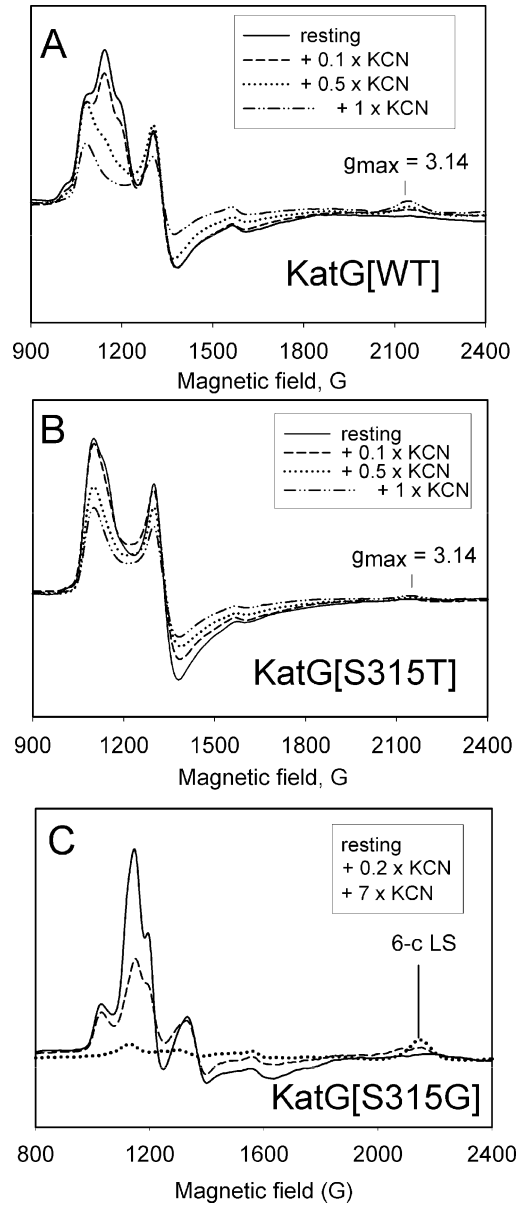

FIGURE 5: Low-temperature EPR spectra of wild-type KatG (A), KatG[S315T] (B), and KatG[S315G] (C) in the presence of increasing molar ratios of cyanide. WT KatG was freshly isolated; KatG[S315T] had been stored for 1 month and KatG[S315G] for two months before treatment with cyanide. Experimental conditions: temperature, 4 K; microwave power, 1 mW; modulation amplitude, 4 G; frequency, 9.3867 GHz.

DISCUSSION

Favored binding of cyanide and peroxide to a 6-c heme iron species in *Mtb* KatG in the presence of the majority 5-c heme species has been illustrated in a variety of approaches. The 6-c and 5-c species are not in equilibrium on the time scale of the ligand binding or titration experiments since ligation of 6-c heme did not perturb the concentration of 5-c species. Biphasic ligand binding had been noted before for *Synechocystis* KatG mutants and in yeast CcP (both WT and certain mutants), but heme heterogeneity was either absent (as for CcP) or was not considered to have any particular importance in any of those cases (*11, 31*−*36*). Here, part of the origin of heterogeneity in ligand binding is assigned to differences in affinity and on-rates for ligand association for 5- and 6-c heme species

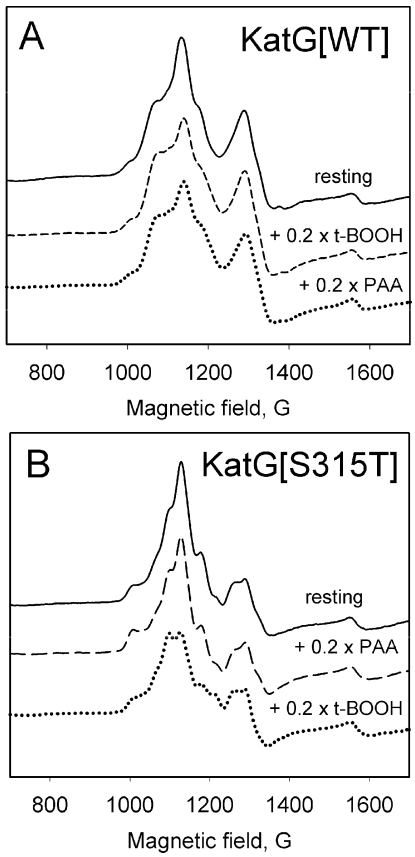

FIGURE 6: Effect of 0.2 mol equiv of peroxides on the low-temperature EPR spectra of "aged" wild-type KatG and KatG[S315T]. A reduction in the intensity of the features assigned to signal r_2 is seen in each case. Experimental conditions: temperature, 4 K; microwave power, 1 mW; modulation amplitude, 4 G; frequency, 9.3867 GHz.

contained in the resting enzymes. It seemed possible that the observation of three features in the equilibrium titration experiment using very small aliquots of ligand with WT KatG could have been consistent with separate titration of 6-c heme and the 5-c heme species, but EPR results did not provide clues that this could be analyzed further since we observed that once the 6-c heme signal had disappeared, the remaining species were titrated simultaneously as ligand was added.

The rate-limiting processes in the first phase of peroxidase turnover involve diffusion into the active site and deprotonation of peroxide substrates for which the distal imidazole is the proton acceptor. Thus, HCN binding models parts of the catalytic pathway for H(R)OOH substrates. The 6-c form of KatG had previously been understood to contain a specifically bound water molecule interacting with heme iron, and the crystal structure of *Mtb* KatG from this laboratory provided evidence for the water molecule, although the water closest to iron is localized farther than is typical for heme iron−aqua complexes. Consistent with an atypical 6-c heme structure in KatG are the analogies to 6-c QS heme assigned in the HRPA2−BHA complex. The facilitated ligand binding to 6-c heme would not be expected if the structure contained tightly bound water such that dissociation would be required to allow anion binding. One speculation these observations raises is that QS heme is more closely related to the low-spin heme structure (*37*), and therefore, there may be a lower barrier to the rearrangements of the heme macrocycle accompanying the binding of strong field ligands to such a 6-c species.

The presence of at least three water molecules in the active site of *Mtb* KatG (PDB code 2CCA) can provide one or more of those necessary for facilitating ligand association. Our spectroscopic analyses provide evidence that water is also associated with heme iron for the enzyme in solution at room temperature and in frozen solution. Furthermore, water molecules beyond those found in the active site in 6-c KatG could also play a role in facilitating diffusion of ligand into the active site (*38*), and there are more waters in the substrate access channel in the crystal structure of the WT compared to the S315T mutant enzyme. These waters may add to the rate enhancement for ligand binding in addition to that from a "special" water molecule positioned to facilitate proton transfer from ligand to distal histidyl imidazole within the active site.

The finding that the 6-c forms of WT and S315T have k_{on} rates for cyanide binding that are 1000-fold faster than the rates for the binding in the secondary process that involves exclusively 5-c heme reveals the importance of the water unless there are additional conformational and or structural differences between the 5-c and 6-c enzyme forms that favor ligand access and binding. We recently reported that INH binding to KatG was more favorable for 6-c KatG (*39*). Then, water molecules preloaded into the active site and the nearby substrate access channel in 6-c KatG can be responsible for the favored ligand and drug binding. In a very extensive analysis of ligand binding (azide and cyanide) to 6-c metmyoglobins, distal side water molecules in addition to the sixth ligand water molecule were also considered to be an enhancing factor in certain examples, consistent with the observations on KatG (*40*).

The steric effect introduced by the methyl group of the threonine replacement of serine in KatG[S315T] might have been expected to introduce a strong interference with ligand binding, yet the mutant exhibited a k_{on} for the first binding phase in aged mutant enzyme close to that for WT KatG. Thus, the barrier to ligand binding presented by the steric effects of the threonine methyl group is overcome by the enhancement due to the presence of water. For the 5-c form of the S315T mutant, ligand association is strongly inhibited, however, as is formation of 6-c heme in the normal aging process during which water accumulates in the heme pocket. If the steric effect is not critically important for ligand binding for a small molecule such as HCN, the rearrangements necessary to establish the 6-c LS heme complex may be restricted in S315T, and the obstacle to this rearrangement is already overcome in the 6-c form of the mutant. Then, the mutant not only lacks the water that could facilitate ligand binding but in its 5-c form also contains a barrier to rearrangement/conversion to 6-c. This barrier or constraints most likely involve the hydrogen bonds between the serine or threonine hydroxyl group and the propionate of pyrrole IV (*9*). The interesting observation that KatG[S315G] and S315C, both of which lack the hydroxyl group of residue 315, convert to 6-c heme at a very rapid rate is consistent with these observations. Interestingly, the K_D values for aged KatG[S315G] increased considerably compared to the fresh enzyme (Table 1), further supporting preferential binding of CN to 6-c heme ($K_{D1} \sim 1$ nM, $K_{D2} = 2.7 \times 10^{-6}$ M).

We had proposed, in the absence of the crystal structure of a KatG-INH complex, that the steric effect of the methyl group in KatG [S315T] was a serious obstacle to high-affinity INH binding and the origin of drug resistance in strains carrying this mutant KatG. The recent solution of the structure of a CcP−INH complex provides some confirmation that residue 315 is important for drug binding (*7*) because there is a hydrogen bond involving the pyridine nitrogen of INH, a water molecule, and the backbone carbonyl of Ser315 in the complex. Now it seems that a change in the architecture surrounding the heme edge at residue 315 has a much more specific influence on binding of the drug because, in mutants at this position, the hydrogen bond that involves the pyridine nitrogen could be altered or eliminated, thereby changing binding affinity.

While there are many factors that impact upon ligand binding in KatG, a recent report presents QM/MM calculations addressing compound I formation that illustrates an energetic advantage provided by a specific water molecule in the active site (*41*−*43*). This water is required as a proton transfer mediator between peroxide and the distal histidine in the first steps of peroxide binding. For monofunctional catalases, however, the active site supposedly expels water when peroxide enters, and the heme functions in a "dry" state that favors two-electron rather than single-electron reactions. It has also been proposed that, in peroxidases (most of which contain 5-c heme as isolated), "a single water molecule enters the active site from the surface of the protein and mediates the deprotonation event at a low barrier and then leaves and peroxidases function with a 'wet' active site. The water also enhances the acidity of H_2O_2 by many orders of magnitude" (*41*). For KatG, which must accommodate both peroxidase and catalase activity in a single active site, it is reasonable that unique structural features are required to allow a catalase-like reaction within a peroxidase active site. Preliminary evidence for the involvement of a novel radical intermediate during catalase turnover has been observed by us (J. Suarez, K. Ranguelova, and R. S. Magliozzo, unpublished observations), which may solve the problem in catalase−peroxidases that must use a "wet" active site, which favors single electron processes, for catalase turnover.

Issues concerning the structure and properties of overexpressed KatG compared to that of KatG *in vivo* are important for establishing an understanding of the physiological functions of this enzyme in *Mtb*. The rate of turnover of KatG in the very slow growing TB cells is reportedly slow (*44*), and a 6-c heme form of KatG is found in the enzyme purified from *Mtb* cultures (*12*). Therefore, this species is a physiologically relevant enzyme form. Here, we have begun to address how the heterogeneous heme species in resting KatG are associated with unique functional properties.

SUPPORTING INFORMATION AVAILABLE

Titration of KatG[S315G] and KatG[S315C] with potassium cyanide, observed rates for cyanide binding to WT KatG and KatG[S315T] as a function of potassium cyanide concentration, and titration of fresh WT KatG and KatG[S315T] with minimal fractional equivalents of potassium cyanide. This material is available free of charge via the Internet at http://pubs.acs.org.

REFERENCES

1. Rouse, D. A., DeVito, J. A., Li, Z., Byer, H., and Morris, S. L. (1996) Site-directed mutagenesis of the katG gene of Mycobacterium tuberculosis: effects on catalase-peroxidase activities and isoniazid resistance. *Mol. Microbiol. 22*, 583–592.
2. Musser, J. M. (1996) Molecular population genetic analysis of emerged bacterial pathogens: selected insights. *Emerg. Infect. Dis. 2*, 1–17.
3. Marttila, H. J., Soini, H., Huovinen, P., and Viljanen, M. K. (1996) katG mutations in isoniazid-resistant Mycobacterium tuberculosis isolates recovered from Finnish patients. *Antimicrob. Agents Chemother. 40*, 2187–2189.
4. Bertrand, T., Eady, N. A. J., Jones, J. N., Jesmin, Nagy, J. M., Jamart-Gregoire, B., Raven, E. L., and Brown, K. A. (2004) Crystal structure of Mycobacterium tuberculosis catalase-peroxidase. *J. Biol. Chem. 279*, 38991–38999.
5. Zhao, X., Yu, H., Yu, S., Wang, F., Sacchettini, J. C., and Magliozzo, R. S. (2006) Hydrogen peroxide-mediated isoniazid activation catalyzed by Mycobacterium tuberculosis catalase-peroxidase (KatG) and its S315T mutant. *Biochemistry 45*, 4131–4140.
6. Yu, S., Girotto, S., Lee, C., and Magliozzo, R. S. (2003) Reduced affinity for isoniazid in the S315T mutant of Mycobacterium tuberculosis KatG is a key factor in antibiotic resistance. *J. Biol. Chem. 278*, 14769–14775.
7. Metcalfe, C., Macdonald, I. K., Murphy, E. J., Brown, K. A., Raven, E. L., and Moody, P. C. (2008) The tuberculosis prodrug isoniazid bound to activating peroxidases. *J. Biol. Chem. 283*, 6193–6200.
8. Pym, A. S., Saint-Joanis, B., and Cole, S. T. (2002) Effect of katG mutations on the virulence of Mycobacterium tuberculosis and the implication for transmission in humans. *Infect. Immun. 70*, 4955–4960.
9. Kapetanaki, S., Chouchane, S., Girotto, S., Yu, S., Magliozzo, R. S., and Schelvis, J. P. (2003) Conformational differences in Mycobacterium tuberculosis catalase-peroxidase KatG and its S315T mutant revealed by resonance Raman spectroscopy. *Biochemistry 42*, 3835–3845.
10. Jakopitsch, C., Auer, M., Ivancich, A., Ruker, F., Furtmuller, P. G., and Obinger, C. (2003) Total conversion of bifunctional catalase-peroxidase (KatG) to monofunctional peroxidase by exchange of a conserved distal side tyrosine. *J. Biol. Chem. 278*, 20185–20191.
11. Jakopitsch, C., Ivancich, A., Schmuckenschlager, F., Wanasinghe, A., Poltl, G., Furtmuller, P. G., Ruker, F., and Obinger, C. (2004) Influence of the unusual covalent adduct on the kinetics and formation of radical intermediates in synechocystis catalase peroxidase: a stopped-flow and EPR characterization of the MET275, TYR249, and ARG439 variants. *J. Biol. Chem. 279*, 46082–46095.
12. Wengenack, N. L., Lane, B. D., Hill, P. J., Uhl, J. R., Lukat-Rodgers, G. S., Hall, L., Roberts, G. D., Cockerill, F. R., III, Brennan, P. J., Rodgers, K. R., Belisle, J. T., and Rusnak, F. (2004) Purification and characterization of Mycobacterium tuberculosis KatG, KatG(S315T), and Mycobacterium bovis KatG(R463L). *Protein Expression Purif. 36*, 232–243.
13. Cardoso, R. F., Cooksey, R. C., Morlock, G. P., Barco, P., Cecon, L., Forestiero, F., Leite, C. Q., Sato, D. N., Shikama Mde, L., Mamizuka, E. M., Hirata, R. D., and Hirata, M. H. (2004) Screening and characterization of mutations in isoniazid-resistant Mycobacterium tuberculosis isolates obtained in Brazil. *Antimicrob. Agents Chemother. 48*, 3373–3381.
14. Loewen, P. C., and Stauffer, G. V. (1990) Nucleotide sequence of katG of Salmonella typhimurium LT2 and characterization of its product, hydroperoxidase I. *Mol. Gen. Genet. 224*, 147–151.
15. Johnsson, K., Froland, W. A., and Schultz, P. G. (1997) Overexpression, purification, and characterization of the catalase-peroxidase KatG from Mycobacterium tuberculosis. *J. Biol. Chem. 272*, 2834–2840.
16. Chouchane, S., Lippai, I., and Magliozzo, R. S. (2000) Catalase-peroxidase (Mycobacterium tuberculosis KatG) catalysis and isoniazid activation. *Biochemistry 39*, 9975–9983.
17. Zhou, Y., Bowler, B. E., Lynch, K., Eaton, S. S., and Eaton, G. R. (2000) Interspin distances in spin-labeled metmyoglobin variants determined by saturation recovery EPR. *Biophys. J. 79*, 1039–1052.
18. Aasa, R., and Vanngard, T. (1975) EPR signal intensity and powder shapes: A reexamination. *J. Magn. Reson. 19*, 308–315.
19. Wengenack, N. L., Todorovic, S., Yu, L., and Rusnak, F. (1998) Evidence for differential binding of isoniazid by Mycobacterium tuberculosis KatG and the isoniazid-resistant mutant KatG(S315T). *Biochemistry 37*, 15825–15834.

20. Abe, M., Kitagawa, T., and Kyogoku, Y. (1978) Resonance Raman spectra of octaethylporphyrinato-Ni(II) and *meso*-deuterated and ^{15}N substituted derivatives. II. A normal coordinate analysis. *J. Chem. Phys. 69*, 4526–4534.
21. Choi, S., Lee, J. J., Wei, Y. H., and Spiro, T. G. (1983) *J. Am. Chem. Soc. 105*, 3692–3707.
22. Choi, S., and Spiro, T. G. (1983) *J. Am. Chem. Soc. 105*, 3683–3692.
23. Heering, H. A., Jansen, M. A., Thorneley, R. N., and Smulevich, G. (2001) Cationic ascorbate peroxidase isoenzyme II from tea: structural insights into the heme pocket of a unique hybrid peroxidase. *Biochemistry 40*, 10360–10370.
24. Chouchane, S., Girotto, S., Kapetanaki, S., Schelvis, J. P., Yu, S., and Magliozzo, R. S. (2003) Analysis of heme structural heterogeneity in Mycobacterium tuberculosis catalase-peroxidase (KatG). *J. Biol. Chem. 278*, 8154–8162.
25. Kapetanaki, S. M., Chouchane, S., Yu, S., Magliozzo, R. S., and Schelvis, J. P. (2005) Resonance Raman spectroscopy of Compound II and its decay in Mycobacterium tuberculosis catalase-peroxidase KatG and its isoniazid resistant mutant S315T. *J. Inorg. Biochem. 99*, 1401–1406.
26. Indiani, C., Feis, A., Howes, B. D., Marzocchi, M. P., and Smulevich, G. (2000) Benzohydroxamic acid-peroxidase complexes: spectroscopic characterization of a novel heme spin species. *J. Am. Chem. Soc. 122*, 7368–7376.
27. Howes, B. D., Schiodt, C. B., Welinder, K. G., Marzocchi, M. P., Ma, J. G., Zhang, J., Shelnutt, J. A., and Smulevich, G. (1999) The quantum mixed-spin heme state of barley peroxidase: A paradigm for class III peroxidases. *Biophys. J. 77*, 478–492.
28. Smulevich, G., Feis, A., Indiani, C., Becucci, M., and Marzocchi, M. P. (1999) Peroxidase-benzhydroxamic acid complexes: spectroscopic evidence that a Fe-H_2O distance of 2.6 Å can correspond to hexa-coordinate high-spin heme. *J. Biol. Inorg. Chem. 4*, 39–47.
29. Jentzen, W., Ma, J. G., and Shelnutt, J. A. (1998) Conservation of the conformation of the porphyrin macrocycle in hemoproteins. *Biophys. J. 74*, 753–763.
30. Maltempo, M. M., Moss, T. H., and Cusanovich, M. A. (1974) Magnetic studies on the changes in the iron environment in chromatium ferricytochrome *c′*. *Biochim. Biophys. Acta 342*, 290–305.
31. Obinger, C., Regelsberger, G., Strasser, G., Burner, U., and Peschek, G. A. (1997) Purification and characterization of a homodimeric catalase-peroxidase from the cyanobacterium Anacystis nidulans. *Biochem. Biophys. Res. Commun. 235*, 545–552.
32. Engleder, M., Regelsberger, G., Jakopitsch, C., Furtmuller, P. G., Ruker, F., Peschek, G. A., and Obinger, C. (2000) Nucleotide sequence analysis, overexpression in Escherichia coli and kinetic characterization of Anacystis nidulans catalase-peroxidase. *Biochimie 82*, 211–219.
33. Erman, J. E. (1974) Kinetic and equilibrium studies of cyanide binding by cytochrome *c* peroxidase. *Biochemistry 13*, 39–44.
34. Bidwai, A., Witt, M., Foshay, M., Vitello, L. B., Satterlee, J. D., and Erman, J. E. (2003) Cyanide binding to cytochrome *c* peroxidase (H52L). *Biochemistry 42*, 10764–10771.
35. Foshay, M. C., Vitello, L. B., and Erman, J. E. (2004) pH Dependence of heme iron coordination, hydrogen peroxide reactivity, and cyanide binding in cytochrome *c* peroxidase (H52K). *Biochemistry 43*, 5065–5072.
36. Jakopitsch, C., Auer, M., Regelsberger, G., Jantschko, W., Furtmuller, P. G., Ruker, F., and Obinger, C. (2003) Distal site aspartate is essential in the catalase activity of catalase-peroxidases. *Biochemistry 42*, 5292–5300.
37. Indiani, C., Feis, A., Howes, B. D., Marzocchi, M. P., and Smulevich, G. (2000) Effect of low temperature on soybean peroxidase: spectroscopic characterization of the quantum-mechanically admixed spin state. *J. Inorg. Biochem. 79*, 269–274.
38. Jakopitsch, C., Droghetti, E., Schmuckenschlager, F., Furtmuller, P. G., Smulevich, G., and Obinger, C. (2005) Role of the main access channel of catalase-peroxidase in catalysis. *J. Biol. Chem. 280*, 42411–42422.
39. Zhao, X., Yu, S., and Magliozzo, R. S. (2007) Characterization of the binding of isoniazid and analogues to Mycobacterium tuberculosis catalase-peroxidase. *Biochemistry 46*, 3161–3170.
40. Brancaccio, A., Cutruzzola, F., Allocatelli, C. T., Brunori, M., Smerdon, S. J., Wilkinson, A. J., Dou, Y., Keenan, D., Ikeda-Saito, M., Brantley, R. E., Jr., et al. (1994) Structural factors governing azide and cyanide binding to mammalian metmyoglobins. *J. Biol. Chem. 269*, 13843–13853.
41. Derat, E., Shaik, S., Rovira, C., Vidossich, P., and Alfonso-Prieto, M. (2007) The effect of a water molecule on the mechanism of formation of compound 0 in horseradish peroxidase. *J. Am. Chem. Soc. 129*, 6346–6347.
42. Jones, P., and Dunford, H. B. (2005) The mechanism of Compound I formation revisited. *J. Inorg. Biochem. 99*, 2292–2298.
43. Jones, P. (2001) Roles of water in heme peroxidase and catalase mechanisms. *J. Biol. Chem. 276*, 13791–13796.
44. Rao, P. K., Roxas, B. A., and Li, Q. (2008) Determination of global protein turnover in stressed mycobacterium cells using hybrid-linear ion trap-fourier transform mass spectrometry. *Anal. Chem. 80*, 396–406.

BI801511U